RIMS Kôkyûroku Bessatsu **B3**
(2007), 025–041

Bifurcation and spatio-temporal evolution of thermal convection patterns in the presence of avoided crossing of neutral stability curves

By

Yuki KATO *

Abstract

Rayleigh–Bénard convection is considered in a rectangular channel with finite aspect ratio, where the linear neutral stability curves exhibit avoided crossings on the Rayleigh number–aspect ratio plane. To examine the effects of the avoided crossings on a nonlinear stage, we derive and analyze weakly nonlinear amplitude equations and envelope equations. Analysis of the amplitude equations reveals that certain nonlinear steady solutions, realized under the crossing of neutral stability curves, are split into two groups in the presence of avoided crossings. The split branches form a folded branch that is qualitatively the same as solutions in a fully nonlinear system. Analysis of the envelope equations suggests that some of the steadily progressive solutions that exist when the neural curves cross, cannot exist in the presence of avoided crossings.

§ 1. Introduction

In linear eigenvalue problems with parameters, two eigenvalues often cross or avoid crossing (Fig. 1). An avoided crossing, also called as a repulsion of eigenvalues, is related to the symmetry of a system [1] and has been observed in many fields. Examples include energy levels in diatomic molecules [2], frequencies of oscillating bubbles [3], transition parameter in superconducting rings [4], and Rayleigh number in thermal convection in rectangular channels [5, 6, 7].

In this study we consider the last example. In Rayleigh–Bénard convection, the linear stability of the conduction state is formulated as an eigenvalue problem. The neutral Rayleigh number Ra can be obtained as eigenvalues that are parameterized by the aspect ratio of the channel As (= width/height). As shown in Fig. 2, the neutral

2000 Mathematics Subject Classification(s): 76R10, 76E06
*Department of Applied Mathematics and Physics, Tottori University, Tottori 680-8552, Japan.

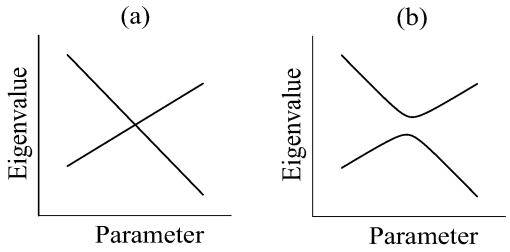

Figure 1. (a) Crossing and (b) avoided crossing of two eigenvalues.

stability curves either cross or avoid crossing depending on the number of convection rolls.

In this paper, we investigate how the avoided crossing of the linear neutral curves affects the convection rolls in a nonlinear stage. We first show that steady convection rolls in a channel with rigid sidewalls form folded solution branches due to the avoided crossing of the linear neutral curves. This is an extension of the work reported in Ref. [8]. We next show the spatio-temporal evolution of the rolls with and without avoided crossings.

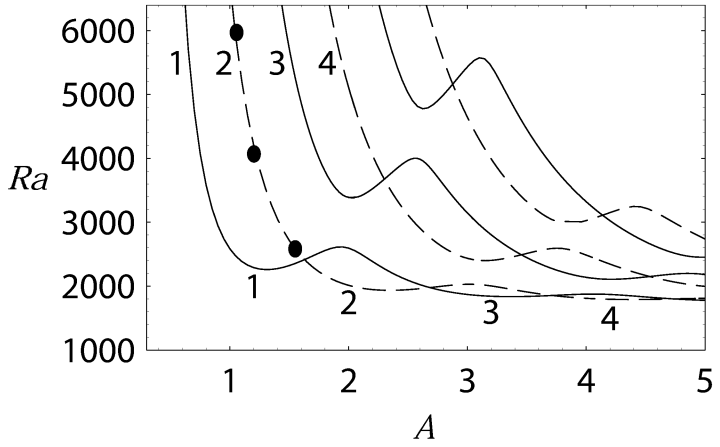

Figure 2. Linear neutral stability curves for longitudinal convection rolls aligned parallel to the sidewalls of a rectangular channel, based on the first six eigenvalues. The numbers indicate the number of rolls. Curves for odd and even numbers of rolls are represented by solid and dashed lines, respectively. Crossing is seen for curves with different parity, that is, an odd number of rolls curve and an even number of rolls curve, while curves with the same parity avoid crossing.

§ 2. Basic equations and steady solutions

§ 2.1. Basic equations

We consider the motion of a Boussinesq fluid in an infinitely long channel with a rectangular cross section uniformly heated from below. We consider a through-flow $\bar{U}$ faster than a certain threshold. When the temperature difference between the top and bottom walls is greater than a critical value, two-dimensional steady convection rolls are formed, aligned parallel to the flow [9]. They are called longitudinal rolls. Note that for a through-flow slower than the threshold, three dimensional unsteady convection is established, which is periodic in the streamwise direction. We focus on the longitudinal rolls in the present paper.

The deviation of the velocity $\boldsymbol{u} = (u, v, w)$, pressure p, and temperature θ from the conduction state with the through-flow satisfies

$$\nabla \cdot \boldsymbol{u} = 0, \tag{2.1a}$$

$$\boldsymbol{u}_t + \bar{U}\boldsymbol{u}_x + (v\bar{U}_y + w\bar{U}_z)\boldsymbol{e}_x + (\boldsymbol{u}\cdot\nabla)\boldsymbol{u} = -\nabla p + Pr\nabla^2\boldsymbol{u} + PrRa\theta\boldsymbol{e}_z, \tag{2.1b}$$

$$\theta_t + \bar{U}\theta_x + wT_z + (\boldsymbol{u}\cdot\nabla)\theta = \nabla^2\theta, \tag{2.1c}$$

where $\boldsymbol{e}_x$ and $\boldsymbol{e}_z$ are unit vectors in the streamwise and vertical direction, respectively. All the variables are non-dimensional. The characteristic length, time, and temperature are the height of the channel h, the thermal diffusive time h^2/κ, and the temperature difference ΔT between the top and bottom walls, where κ is the thermal diffusivity. The Rayleigh number Ra and Prandtl number Pr are defined by

$$Ra = \alpha\Delta T g h^3/(\nu\kappa), \qquad Pr = \nu/\kappa,$$

where α is the coefficient of cubical expansion, g is the gravitational acceleration, and ν is the kinematic viscosity. We define the Reynolds number by using the maximum value of the flow U_{max}, $Re = U_{max}h/\nu$. The non-dimensional through-flow is written as $\bar{U} = RePrU(y,z)$. Here, U satisfies $U_{yy} + U_{zz} = \text{const.}$ and the maximum value of U is equal to unity. We impose the non-slip condition $\boldsymbol{u} = \boldsymbol{0}$ on the rigid boundaries $z = \pm 1/2$ and $y = \pm As/2$, where As is the aspect ratio (width/height) of the cross section of the channel. The sidewalls at $y = \pm As/2$ are assumed to be perfectly insulating, satisfying $\theta_y = 0$.

The longitudinal rolls are steady and uniform in the streamwise direction. We can therefore introduce the stream function by $v = \psi_z$ and $w = -\psi_y$. Eliminating the pressure terms in (2.1) and neglecting the time dependency, we have a closed form of the equations for the stream function $\psi(y,z)$ and the temperature $\theta(y,z)$:

$$\nabla^4\psi - Ra\theta_y + Pr^{-1}J(\psi, \nabla^2\psi) = 0, \tag{2.2a}$$

$$\nabla^2\theta - \psi_y + J(\psi, \theta) = 0, \tag{2.2b}$$

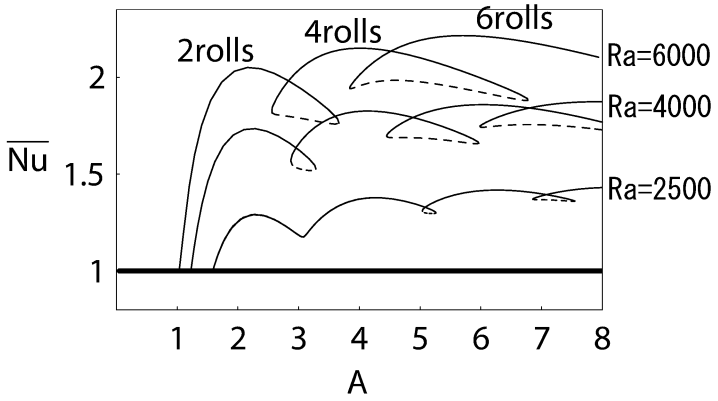

Figure 3. Solutions of (2.2) for rigid sidewalls. The solid lines denote stable branches with respect to a two-dimensional infinitesimal disturbance. The dashed lines show unstable branches.

where $\nabla^2 = \partial_{yy} + \partial_{zz}$ and $J(f,g) = f_y g_z - f_z g_y$. The boundary conditions are now $\psi = \psi_y = \theta_y = 0$ at $y = \pm As/2$ and $\psi = \psi_z = \theta = 0$ at $z = \pm 1/2$.

The roll solutions bifurcating from the trivial solution are even number of rolls or odd number of rolls. To focus on the avoided crossings, we only consider rolls with the same parity hereafter.

§ 2.2. Bifurcation of steady solutions

We solve (2.2) numerically by using the Chebyshev spectral method. Solution branches for even numbers of rolls are shown in Fig. 3. The ordinate in the figure denotes the average value of the Nusselt number, where the Nusselt number is given by

$$Nu(y) = 1 - \theta_z(y, \pm 1/2). \tag{2.3}$$

We have $\bar{Nu} = 1$ for the conduction state, whereas the convection rolls give $\bar{Nu} > 1$. Three bifurcation points of the steady solution are shown as dots on the neutral curve in Fig. 2 for $Ra = 2500$, 4000, and 6000.

When Ra is higher than the critical value, the branches are folded with several loops. Along each loop, the convection pattern changes from n rolls to $n+2$ rolls. We note that crossings of two branches in this figure are not bifurcation points.

In §4, we show that the folded branches can be explained by considering the avoided crossing of the neutral curves. To that end, we derive amplitude equations in the presence of avoided crossings in the next section.

§ 3. Derivation of amplitude equations and envelope equations

The amplitude equations in the presence of avoided crossings have been derived in Ref. [8]. Here, we derive the envelope equations of n rolls and $n+2$ rolls for later use.

The amplitude equations can then be derived from the envelope equations by neglecting spatial changes of the amplitude.

The derivation of the amplitude or envelope equations from the basic equations requires a double zero bifurcation point of n and $n+2$ rolls. To this end, we introduce somewhat artificial boundary conditions:

$$\text{(3.1a)}\quad \boldsymbol{u} = \mathbf{0},\ \theta = 0 \quad \text{on} \quad z = \pm 1/2,$$

$$\text{(3.1b)}\quad \delta u \pm (1-\delta)u_y = 0,\ v = 0,\ \delta w \pm (1-\delta)w_y = 0,\ \theta_y = 0 \quad \text{on} \quad y = \pm As/2.$$

For $\delta = 0$, we have stress-free conditions on $y = \pm As/2$. In this case, the functions $\boldsymbol{u}$ and θ can be extended to periodic functions with a period of $2As$ in the lateral direction. All the neutral curves then cross irrespective of the number of rolls and we have crossover points of n and $n+2$ rolls. For $\delta \neq 0$, the problem cannot be extended to the periodic case and the neutral curves of the same parity avoid crossing. For $\delta = 1$, the non-slip conditions imposed in the previous section are restored.

We rewrite the basic equations (2.1) and boundary conditions (3.1) as

$$S\partial_t \Phi + L\Phi + N(\Phi, \Phi) = 0 \quad \text{and} \quad B\Phi = 0. \tag{3.2}$$

Here, $\Phi = (p, u, v, w, \theta)$, S is a unit matrix whose diagonal component in the first row is replaced by zero, and $L\Phi$ and $N(\Phi, \Phi)$ are linear and nonlinear terms, respectively.

We assume that the neutral curves for n and $n+2$ rolls cross at $(As, Ra) = (As^*, Ra^*)$ for $\delta = 0$. We consider the neighborhood of the crossover point:

$$As = As^* + \epsilon^2 \tilde{A}, \quad Ra = Ra^* + \epsilon^2 \tilde{R}, \quad \delta = \epsilon^2 \tilde{\delta}, \tag{3.3}$$

where ϵ is a small parameter. We expand Φ,

$$\Phi = \epsilon \Phi_1 + \epsilon^2 \Phi_2 + \epsilon^3 \Phi_3 + \cdots, \tag{3.4}$$

where $\Phi_j = \Phi_j(t_1, t_2, \cdots, x_1, x_2, \cdots, y, z)$, $t_n = \epsilon^{2n} t$, and $x_n = \epsilon^n x$.

Substituting (3.3) and (3.4) into (3.2), we have a linear eigenvalue problem in $O(\epsilon)$. The eigenvalue is Ra^*, listed in Table 1, and the eigenfunctions are

$$\Phi_1 = a_1 \Psi_n + b_1 \Psi_{n+2}, \tag{3.5}$$

where $\Psi_n(y, z)$ and $\Psi_{n+2}(y, z)$ represent n rolls and $n+2$ rolls, respectively. The amplitudes a_1 and b_1 are real and depend on t and x. It should be noted that Ra^* is higher than the neutral Ra of $n+1$ rolls. To obtain (3.5), we restrict eigenfunctions to ones with a certain symmetry which characterizes even rolls or odd rolls and neglect $n+1$ rolls.

Table 1. Crossover points of n rolls and $n+2$ rolls for $\delta = 0$. Ra^* and As^* are independent of Pr and Re.

n	Ra^*	As^*
1	2573	1.82
2	2022	2.90
3	1873	3.94
4	1811	4.97

We substitute (3.5) into the equations obtained in $O(\epsilon^2)$. The solvability conditions of the equations of $O(\epsilon^2)$ give

$$\partial_{t_1} a_1 + c_n \partial_{x_1} a_1 = 0 \quad \text{and} \quad \partial_{t_1} b_1 + c_{n+2} \partial_{x_1} b_1 = 0, \tag{3.6}$$

where c_n and c_{n+2} are the phase velocities for n rolls and $n+2$ rolls, which can be calculated using Ψ_n and Ψ_{n+2} . Under these conditions, we get Φ_2 as functions of Φ_1 and $\partial_{x_1}\Phi_1$. Finally, we substitute Φ_1 and Φ_2 into the equations of $O(\epsilon^3)$. The solvability conditions of the resultant equations yield

$$\begin{aligned}(\partial_{t_1} a_2 + \partial_{t_2} a_1) + c_n(\partial_{x_1} a_2 + \partial_{x_2} a_1) + d_n \partial_{x_1 x_1} a_1 \\ +\lambda_1 a_1 + \lambda_2 b_1 + \mu_1 a_1^3 + \mu_2 a_1 b_1^2 = 0,\end{aligned} \tag{3.7a}$$

$$\begin{aligned}(\partial_{t_1} b_2 + \partial_{t_2} b_1) + c_{n+2}(\partial_{x_1} b_2 + \partial_{x_2} b_1) + d_{n+2} \partial_{x_1 x_1} b_1 \\ +\lambda_3 a_1 + \lambda_4 b_1 + \mu_3 a_1^2 b_1 + \mu_4 b_1^3 = 0.\end{aligned} \tag{3.7b}$$

We introduce the new variables

$$\begin{aligned}A(t_1, t_2, \cdots, x_1, x_2, \cdots) &= \epsilon a_1 + \epsilon^2 a_2 + \cdots, \\ B(t_1, t_2, \cdots, x_1, x_2, \cdots) &= \epsilon b_1 + \epsilon^2 b_2 + \cdots\end{aligned}$$

and return to the original scale of t and x. From (3.6) and (3.7), we get the envelope equations

$$A_t + c_n A_x + d_n A_{xx} + \lambda_1 A + \lambda_2 B + \mu_1 A^3 + \mu_2 A B^2 = 0, \tag{3.8a}$$

$$B_t + c_{n+2} B_x + d_{n+2} B_{xx} + \lambda_3 A + \lambda_4 B + \mu_3 A^2 B + \mu_4 B^3 = 0. \tag{3.8b}$$

Here, $\lambda_1 = \lambda_{n,R} dR + \lambda_{n,A} dA + \delta_{n,n}\delta$ and $\lambda_2 = \delta_{n,n+2}\delta$, where $dR = Ra - Ra^*$ and $dA = As - As^*$ are deviations from the crossover point. λ_3 and λ_4 have the same form as λ_2 and λ_1, respectively, in which n and $n+2$ are replaced by $n+2$ and n, respectively. We note that (3.8) are valid only for $n \geq 2$. For $n = 1$, an additional term A^3 must be included in (3.8b) due to a 1:3 resonance.

Table 2. Coefficients in (3.8) and (3.9) for $n = 2$, $Pr = 0.71$, and $Re = 60$.

$c_n = 31.7,\ \ d_n = -0.77,\ \ c_{n+2} = 33.3,\ \ d_{n+2} = -0.97$
$\lambda_{n,R} = -0.0047,\ \ \lambda_{n,A} = 2.8,\quad \lambda_{n+2,R} = -0.0073,\ \ \lambda_{n+2,A} = -5.4$
$\delta_{n,n} = 0.096,\ \ \delta_{n,n+2} = 0.17,\ \ \delta_{n+2,n} = 0.17,\ \ \delta_{n+2,n+2} = 0.29$
$\mu_1 = 0.016,\ \ \mu_2 = 0.048,\ \ \mu_3 = 0.051,\ \ \mu_4 = 0.036$

Linear terms including δ represent the effect of the aperiodicity of the boundary conditions in the y direction. In particular, the two terms $\lambda_2 B$ and $\lambda_3 A$ are essential for avoided crossings.

Note that all the coefficients in (3.8) are real. The coefficients of A_x, A_{xx}, B_x, and B_{xx}, that is c_n, c_{n+2}, d_n, and d_{n+2}, depend on Re and Pr. The coefficients of the other linear terms are independent of Re and Pr, and the coefficients of the nonlinear terms are independent of Re and depend only on Pr. We calculate all the coefficients numerically, for $n = 2$, 3, 4, 5, 6 and $Pr = 0.001$–1000. Four coefficients of the nonlinear terms are positive and $D \equiv \mu_1\mu_4 - \mu_2\mu_3 < 0$. We list the coefficients for $n = 2$, $Pr = 0.71$, and $Re = 60$ in Table 2.

When we neglect the spatial dependence of A and B in (3.8), we obtain the following amplitude equations:

$$A_t + \lambda_1 A + \lambda_2 B + \mu_1 A^3 + \mu_2 A B^2 = 0, \tag{3.9a}$$

$$B_t + \lambda_3 A + \lambda_4 B + \mu_3 A^2 B + \mu_4 B^3 = 0. \tag{3.9b}$$

§ 4. Steady solution of amplitude equations

We examine the relation between the avoided crossing of the linear neutral curves and the folded branches of the nonlinear steady solutions (shown in Fig. 3), based on the amplitude equations (3.9). In Ref. [8], we suggest that a simplified version of (3.9) can be used to explain the folded branches. Here, we confirm this by using the coefficients in Table 2, which are consistent with the basic equations of fluid motion.

We investigate bifurcation of the equilibrium solutions to (3.9) for $\delta = 0$ and $\delta \neq 0$. For $\delta = 0$, the neutral curves cross in the dA–dR plane. In this case, we have four types of equilibrium solutions: (i) trivial solution $A = B = 0$, (ii) pure mode $A \neq 0$, $B = 0$ (A-mode), (iii) pure mode $A = 0$, $B \neq 0$ (B-mode), (iv) mixed mode $A \neq 0$, $B \neq 0$ (M-mode). The dA dependence of the norm of these solutions is shown in Fig. 4(a).

Two pure modes bifurcate from the trivial solution. The mixed mode arises by secondary bifurcation from pure modes. When the four coefficients μ_j are positive, the

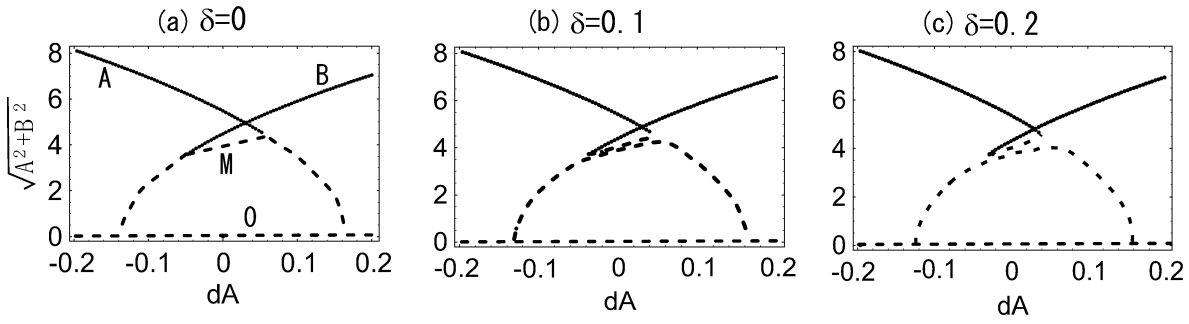

Figure 4. Equilibrium solutions to (3.9) for $dR = 100$. The solid lines denote stable branches and the dashed lines denote unstable branches. A, B, M, and 0 denote the A-mode, B-mode, M-mode, and trivial solutions, respectively.

mixed mode is stable for $D = \mu_1\mu_4 - \mu_2\mu_3 > 0$ and unstable for $D < 0$. Based on the coefficients in Table 2, the mixed mode is confirmed to be unstable.

We next consider nonzero δ, which yields avoided crossing of the linear neutral curves. For $\delta \neq 0$, there are no pure modes. However, we name the solutions for $\delta \neq 0$ based on those for $\delta = 0$, that is, for instance, when a solution for $\delta \neq 0$ originates from the A-mode for $\delta = 0$, we call it the A-mode.

We show bifurcation diagrams for $\delta = 0.1$, 0.2 in Fig. 4(b), (c). When $\delta \neq 0$, the mixed mode splits into two groups and connects with the A-mode or B-mode. This is because the pitchfork bifurcation of the mixed mode is structurally unstable. As a result, the upper branch forms a loop. The equilibrium solutions of the amplitude equations for $\delta \neq 0$ qualitatively agree with the solutions of the fully nonlinear system for $\delta = 1$ (Fig. 3). The folded branches with loops are therefore due to the avoided crossing of the neutral curves. In other words, it is due to the aperiodicity of the boundary conditions in the lateral direction.

§ 5. Spatio-temporal evolution

In this section, we consider the spatio-temporal evolution of the rolls by using the envelope equations (3.8). Our main interest is whether the avoided crossing also affects the spatial structure of the rolls, especially when two modes are stable simultaneously.

We introduce a moving frame $x' = x - Vt$ with mean velocity of the A-mode and B-mode of $V = (c_n + c_{n+2})/2$. In this frame, the equations (3.8) are rewritten as

$$A_t - cA_x + d_nA_{xx} + \lambda_1 A + \lambda_2 B + \mu_1 A^3 + \mu_2 AB^2 = 0, \tag{5.1a}$$

$$B_t + cB_x + d_{n+2}B_{xx} + \lambda_3 A + \lambda_4 B + \mu_3 A^2 B + \mu_4 B^3 = 0, \tag{5.1b}$$

where $c = (c_{n+2} - c_n)/2$ and the prime in x' is omitted.

When $\delta = 0$, or equivalently $\lambda_2 = \lambda_3 = 0$, (5.1) are reduced to a real version of the coupled Ginzburg–Landau equations. It is known that the coupled Ginzburg–Landau equations have a variety of coherent structures including chaos as solutions [10]. A comprehensive analysis of the effects of avoided crossing on the various coherent structures are beyond the scope of this paper. Here, we deal with the structures obtained for the coefficients in Table 2.

§ 5.1. Simulation

We first solve the equations (5.1) numerically. In the x direction, we adopt periodic boundary conditions with a period L for simplicity and use the Fourier-spectral method. We set the parameters $dR = 100$ and $dA = -0.1 \sim 0.1$, for which the A-mode or B-mode are stable (see Fig. 5).

We use several initial conditions, including the A-hump and B-hump and their combination, as shown in Fig. 6. Humps with width $x_2 - x_1$ are given by

$$A(x,0) = \bar{A}\{[1+\tanh r(x-x_1)] - [1+\tanh r(x-x_2)]\}/2, \tag{5.2a}$$

$$B(x,0) = \bar{B}\{[1+\tanh r(x-x_1)] - [1+\tanh r(x-x_2)]\}/2, \tag{5.2b}$$

where $r = 0.4$. Here, $(\bar{A}, \bar{B})$ denotes the equilibrium solution of (3.9), which can be A-mode or B-mode.

Figure 7 shows examples of time evolutions. The spatial structures consist of flat regions and 'fronts' connecting the flat regions. In the flat regions, (A, B) can be A-mode, B-mode or the trivial solution (0,0). We refer to the front connecting the A-mode and (0, 0) as AO. Similarly, we denote the fronts OA, BO, and OB as shown in Fig. 8.

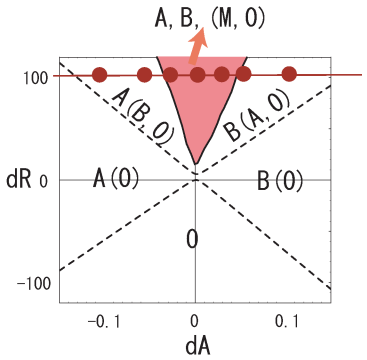

Figure 5. Stability diagram of the equilibrium solution to (3.9) for $\delta = 0.1$. The dashed lines show neutral curves. A, B, M, and 0 without parentheses denote stable solutions and those with parentheses denote unstable solutions. The A-mode and B-mode are stable simultaneously in the grey region. We investigate (5.1) for the points (dA, dR) shown by dots.

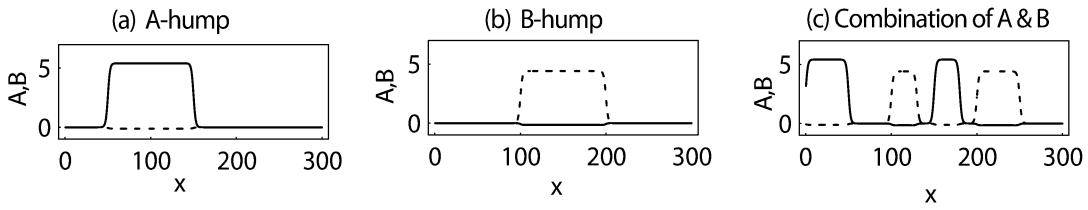

Figure 6. Examples of initial conditions. The solid lines denote A and the dotted lines denote B.

For $\delta = 0$ and $dA = 0.001$, the fronts OA, AO, BO, and OB propagate with almost constant velocity, until two fronts collide or a new flat region $-\bar{B}$ evolves. As $t \to \infty$, almost the whole region is occupied only by $\pm\bar{A}$ or $\pm\bar{B}$ and no combinations of A-mode and B-mode are observed. We should note that the fronts obtained by our simulation are not necessarily stable. When a small disturbance is added to the initial condition, the fronts do not propagate with a constant velocity. Our simulation merely suggests the existence of the front solutions.

For $\delta = 0.1$ and $dA = 0.001$, the fronts OA and BO propagate with a constant velocity, as for $\delta = 0$, whereas the fronts AO and OB are not maintained. Near the front AO, the B-mode grows. Similarly, the A-mode grows near the front OB. As a result, we realized a combination of A-mode (n rolls) and B-mode ($n + 2$ rolls). We examine $dA = \pm 0.1, \pm 0.07, \pm 0.05$ as well as $dA = 0.001$. For these values of dA and $dR = 100$, we did not obtain the fronts AO and OB in the presence of avoided crossings ($\delta \neq 0$) [1]. This suggests that the perturbation δ affects the existence or stability of the front solutions AO and OB. We will discuss the existence of the front solutions in the next subsection.

We now consider the velocity of the fronts. Imposing $\delta = 0$ and $B \equiv 0$ (or $A \equiv 0$), the equations (5.1) are reduced to an uncoupled one-dimensional system that is called the Fisher–Kolmogorov equation. The Fisher–Kolmogorov equation has the front solutions AO or BO as a one parameter family, in which the velocity v is a parameter. For multiple fronts with various velocities, it is known that a selected velocity v^* satisfies a marginal stability hypothesis [11, 12]. That is, there is a natural velocity v^* such that a localized disturbance imposed on the trivial solution gives marginal stability in the moving frame v^*. We calculate v^* giving the marginal stability for a two-dimensional coupled system with $\delta \neq 0$ and compare it with the velocity of the front obtained by the simulation.

We substitute $A, B \propto \exp(\sigma t - kx)$ into the linearized equations of (5.1), giving the dispersion relation $\sigma = \sigma(k)$. The conditions of marginal stability are given by

[1] We have examined time evolution of the A-hump also for $\delta = 0.001, 0.01$ and 0.5, $dA = 0.001$, $dR = 100$. Qualitative results do not depend on the value of δ if $\delta \neq 0$.

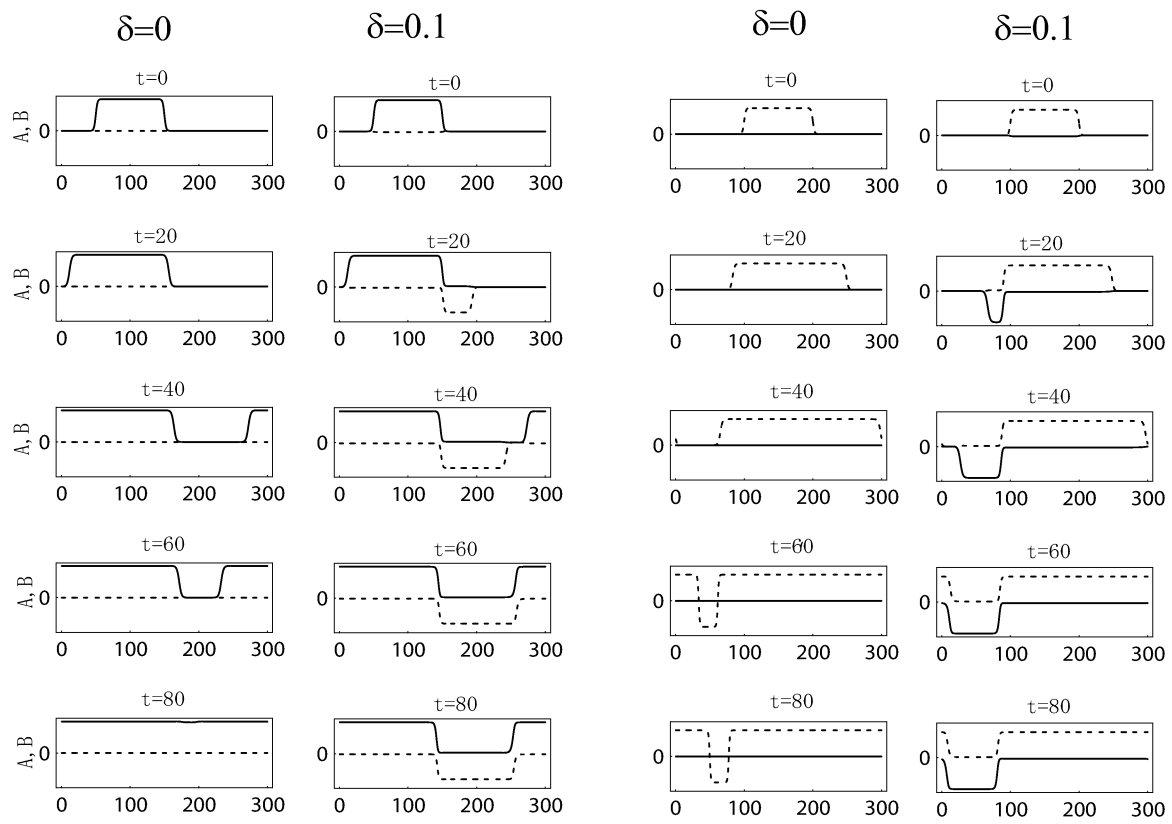

Figure 7. Examples of time evolutions of an A-hump and a B-hump. $dR = 100, dA = 0.001$. The solid and dotted lines denote A and B, respectively.

Figure 8. Names of fronts. The solid and dotted lines denote A and B, respectively.

$\mathrm{Im}(d\sigma/dk) = 0$ and $\sigma/k = d\sigma/dk$. We list the velocities v^* $(= \sigma/k)$ satisfying these conditions in Table 3.

We next estimate the velocity of the fronts obtained by the simulation. As shown in Fig. 7, fronts collide with each other due to the periodic boundary conditions. We measure the velocity v in a short duration before the collision and list it in Table 3. For both $\delta = 0$ and 0.1, v agrees with v^*, giving marginal stability. As far as we examined for $dA \in [-0.1, 0.1]$ the velocities of fronts obtained by the simulation agree with v^*.

Table 3. Velocity v^* corresponding to marginal stability and velocity v of the fronts obtained by the simulation. $dR = 100$ and $dA = 0.001$.

fronts	AO	BO	OA	OB
v^* for $\delta = 0$	0.40	2.49	-2.00	-0.89
v^* for $\delta = 0.1$	0.39	2.46	-1.99	-0.86
v for $\delta = 0$	0.4	2.5	-1.9	-0.9
v for $\delta = 0.1$	—	2.4	-1.9	—

§ 5.2. Front solutions and velocity

We next consider why some fronts are obtained by the simulation in the presence of avoided crossings while other fronts are not. We focus on the fronts AO and BO in this subsection.

We introduce a moving frame $\xi = x - vt$. A steadily progressive front solution with velocity v satisfies the ordinary differential equations

$$-(v+c)A_\xi + d_n A_{\xi\xi} + \lambda_1 A + \lambda_2 B + \mu_1 A^3 + \mu_2 A B^2 = 0, \tag{5.3a}$$

$$-(v-c)B_\xi + d_{n+2} B_{\xi\xi} + \lambda_3 A + \lambda_4 B + \mu_3 A^2 B + \mu_4 B^3 = 0. \tag{5.3b}$$

In this subsection, we impose the boundary conditions

$$(A, B) \to (\bar{A}, \bar{B}) \ \text{ as } \ \xi \to -\infty, \tag{5.4a}$$

$$(A, B) \to (0, 0) \ \text{ as } \ \xi \to \infty, \tag{5.4b}$$

where $(\bar{A}, \bar{B})$ is the A-mode when considering the front AO and the B-mode for front BO.

For $\delta = 0$, we have $\bar{B} = 0$ for the A-mode. Setting $B \equiv 0$ in eqs.(5.3) gives an uncoupled equation for $\delta = 0$

$$(-d_n)A_{\xi\xi} = -(v+c)A_\xi + \lambda_1 A + \mu_1 A^3 \tag{5.5}$$

which has the front solution AO for an arbitrary value of v as long as $v > -c$ [11]. This condition for v is important in a subsequent discussion; we therefore mention an explanation in ref. [11] here.

If we regard ξ as *time* and A as a *position* of a particle whose mass is $-d_n(> 0)$, we can consider (5.5) as an equation of motion of the particle. The first term in the right hand side represents a friction and the second term is a force with a potential $V(A) = -\lambda_1 A^2/2 - \mu_1 A^4/4$. When $\lambda_1 < 0$, the local maximum and minimum of $V(A)$ agree with the A-mode and the trivial solution ($A \equiv 0$), respectively. The front *AO*

thus corresponds to a trajectory starting from the local maximum and falling into the local minimum of the potential. From the mechanical point of view, such a trajectory is always possible if the *damping coefficient* $v + c$ is positive, that is, $v > -c$. Similarly, based on an mechanical argument as above, we conclude that the front BO with $A \equiv 0$ exists for an arbitrary value of $v > c$ for $\delta = 0$.

For $\delta \neq 0$, the question of the existence of the front solution is not trivial. We apply the so-called counting argument [10, 12]. If we introduce the variables $A' \equiv A_\xi$ and $B' \equiv B_\xi$ and view (5.3) as a four-dimensional dynamical system, a front solution is a heteroclinic orbit connecting two fixed points of the dynamical system. The multiplicity of the orbit can be estimated by the dimensions of the unstable manifold of the fixed points. We assume that the dimensions of the unstable manifold of the A-mode and the trivial solution are N_A and N_0, respectively. Here, stability is in the sense of ξ-evolution. Then, the multiplicity of the front solution AO, N, is at most

$$N = N_p + (N_A - 1) - N_0. \tag{5.6}$$

Here, N_p is the number of parameters in (5.3), for which we have $N_p = 1$. Similarly, the multiplicity of the front BO is given by $N = N_p + (N_B - 1) - N_0$.

We examine the linear stability of the fixed points, the A-mode, B-mode, and trivial solution, in the range $-3 < v < 3$. The dimensions of the unstable manifold of the A-mode and B-mode are always $N_A = 2$ and $N_B = 2$, respectively. The dimension of the unstable manifold of the trivial solution depends on v. Figure 9 shows the growth rate s of an infinitesimal disturbance $[(A, B) = (a, b)\exp(s\xi)]$ added to the trivial solution. From the value of s, we see that as $\xi \to \infty$,

$$A \text{ does not tend to 0 for } v < -0.8, \tag{5.7a}$$

$$A \text{ tends to 0, } \begin{cases} \text{oscillatory decay for } -0.8 < v < 0.4, \\ \text{monotonic decay for } 0.4 < v, \end{cases} \tag{5.7b}$$

$$B \text{ does not tend to 0 for } v < 0.8, \tag{5.7c}$$

$$B \text{ tends to 0, } \begin{cases} \text{oscillatory decay for } 0.8 < v < 2.5, \\ \text{monotonic decay for } 2.5 < v. \end{cases} \tag{5.7d}$$

The dimension of the unstable manifold is thus $N_0 = 4$ for $v < -0.8$, $N_0 = 2$ for $-0.8 < v < v_c = 0.8$, and $N_0 = 0$ for $v_c < v$. From the counting argument, we have no solution for $v < -0.8 (N < 0)$. For $-0.8 < v < v_c (N = 0)$, the front solution is expected to be a discrete set. It is therefore highly unlikely that a front with a given velocity exists for $v < v_c$. For $v > v_c$, we have $N = 2$. We expect that the fronts AO and BO exist as a two parameter family.

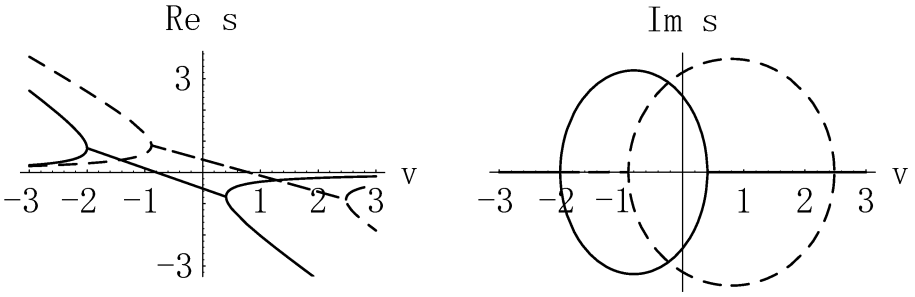

Figure 9. Growth rate s for $dR = 100$, $dA = 0$, and $\delta = 0$. The solid lines denote s of an $a-$component with $b = 0$. The dashed lines are of a $b-$component with $a = 0$. The growth rate for $\delta = 0.1$ agrees with these figures graphically.

To confirm the prediction by the counting argument, we solve the boundary value problem (5.3) with (5.4) numerically for $\delta = 0, 0.1$ and 0.5. We transform the infinite region to a finite region $(-1, 1)$, and expand A and B by the Chebyshev polynomials and use the Newton–Raphson iteration. To avoid an indeterminacy by the translation $x \to x+$constant, we introduce an additional condition: $A(0) = 3$ for the front AO and $B(0) = 3$ for the front BO.

The fronts BO and AO are shown in Fig. 10 and 11 for $\delta = 0, 0.1$. We obtain the front BO for $v > v_c$ and $\delta = 0, 0.1, 0.5$ as a two parameter family, in which the parameters are v and $A(0)$. Whereas for $v < v_c$, we did not obtain the front BO. This is consistent with the counting argument. Note that $v^* = 2.4$ or 2.5, corresponding to the marginal stability, is greater than v_c, that is, the fronts with the velocity v^* exist as solutions to (5.3).

The existence of the front AO depends on δ. For $v > v_c$, we obtain the front solution AO as a two parameter family. When $v < v_c$, we did not obtain the front AO for $\delta = 0.1, 0.5$, as predicted by the counting argument. For $\delta = 0$, we have the front AO even for $v < v_c$. It is because the front AO with $B \equiv 0$ exists for an arbitrary value of $v(> -c)$, as explained above. It is noted that this does not contradict the counting argument. Since an unstable manifold of the A-mode and a stable manifold of the trivial solution coincide for $B \equiv 0$, the multiplicity of the front with $B \equiv 0$ can be greater than the estimate by (5.6).

Figure 11 shows that the perturbation δ narrows the velocity range of AO. In particular, we note that $v^* = 0.4$ is less than v_c. No front solution with v^* exists as a solution to (5.3) for $\delta \neq 0$. This can be related to the fact that no fronts AO were obtained by the simulation in the presence of avoided crossings.

Lastly, we mention the structure of the fronts. We obtain front solutions with an oscillatory tail for low value of v. This is consistent with the statements (5.7), which are given by the linear stability analysis of the trivial solution.

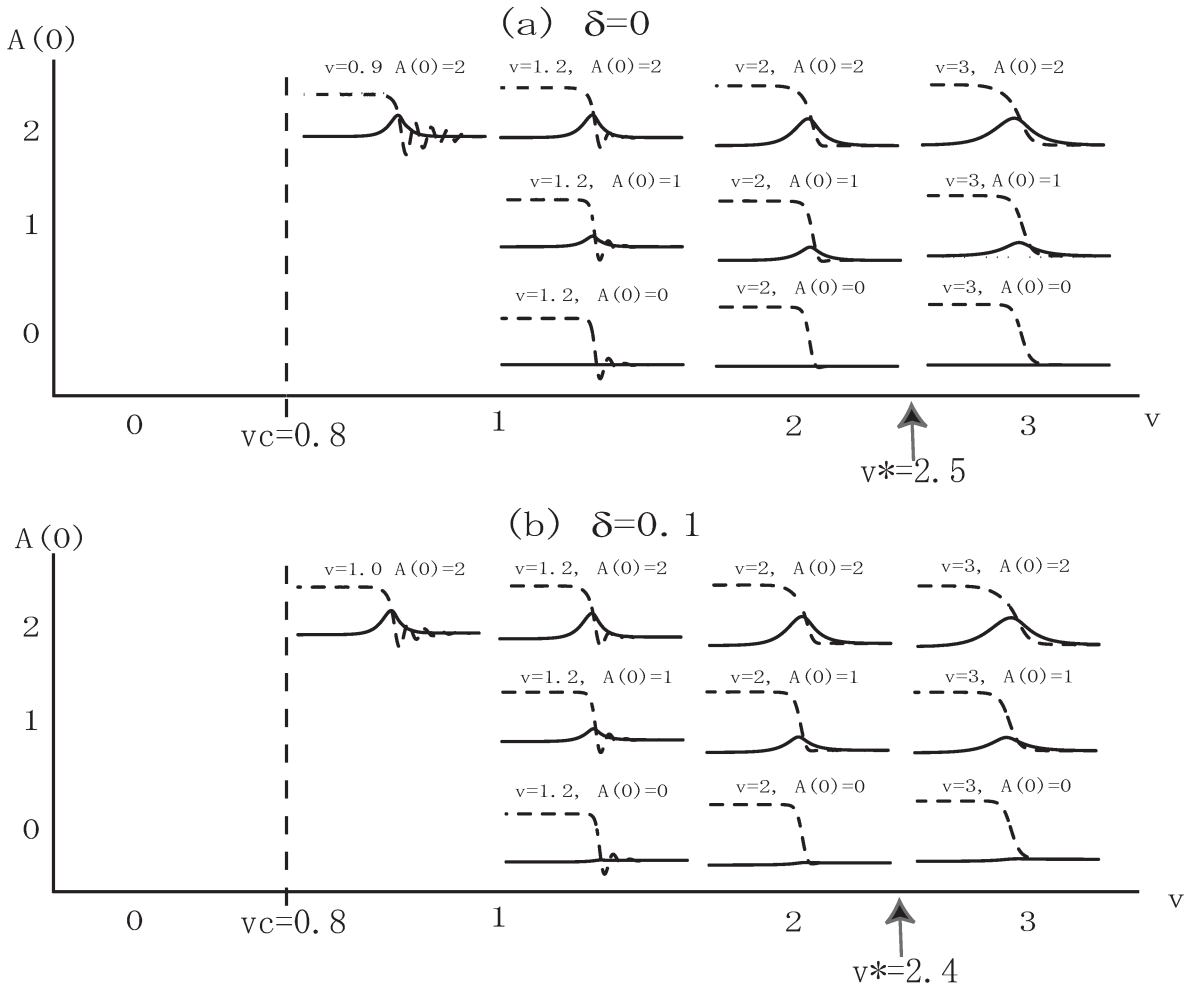

Figure 10. Fronts BO obtained by solving (5.3) and (5.4) for $dR = 100$ and $dA = 0$.

§ 6. Concluding Remarks

We have investigated steady solutions to the fully nonlinear system (2.2) and amplitude equations (3.9), and steadily progressive fronts as solutions to the envelope equations (3.8) and (5.3). The bifurcation characteristics of the steady solutions to the amplitude equations agree with the numerical results of the fully nonlinear system shown in §2. The perturbation δ causes avoided crossing of the linear neutral curves [7] and results in folded branches in the nonlinear stage.

The perturbation also affects the spatio-temporal evolution. In the presence of avoided crossings ($\delta \neq 0$), some of the steadily progressive fronts obtained for $\delta = 0$, AO and OB, are not obtained in the simulation. The perturbation restricts the velocity range of the front solution AO; a front AO with velocity v^* does not exist in the presence of avoided crossings.

Near the front AO (OB), B-mode (A-mode) grows. It suggests that a defect con-

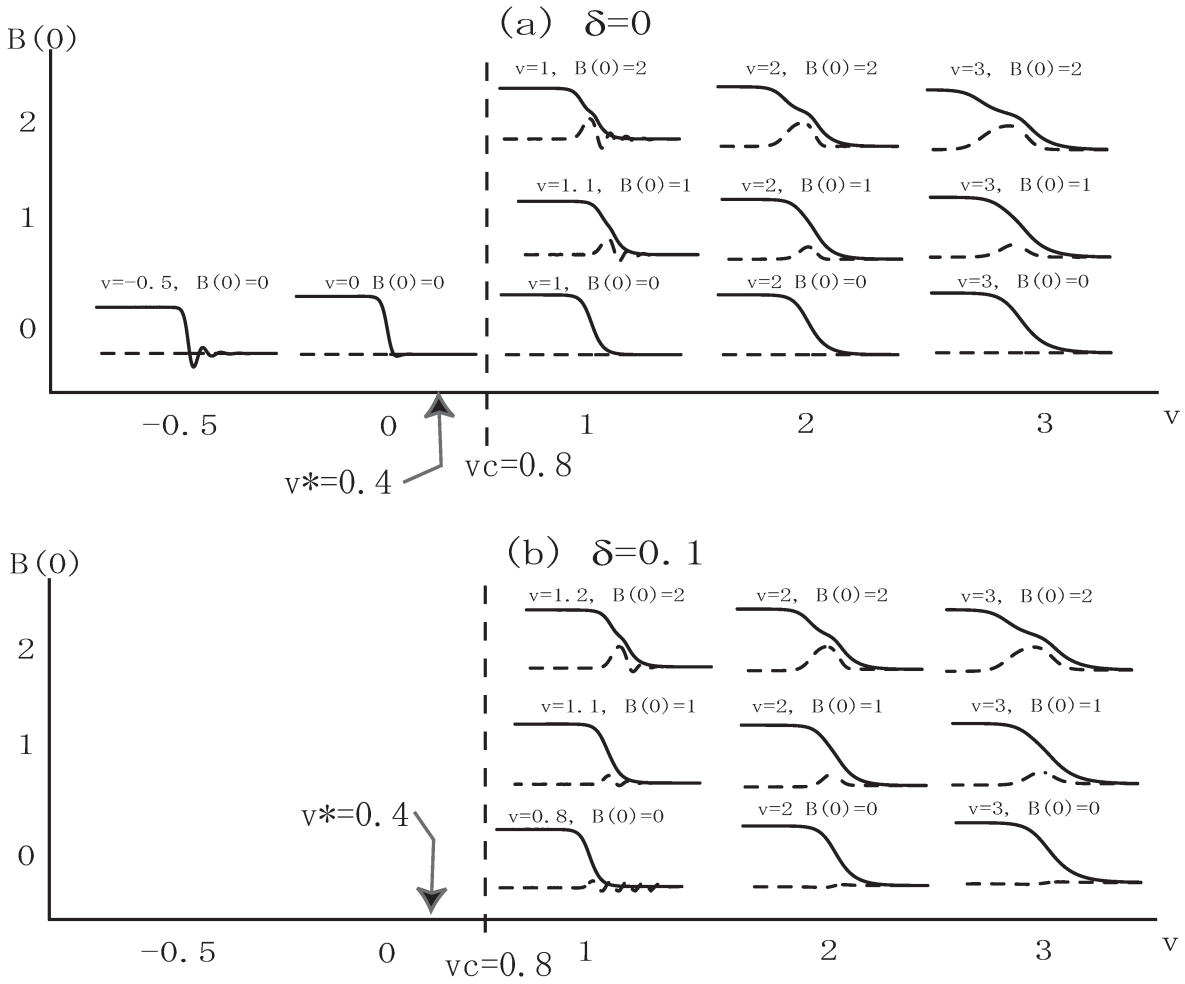

Figure 11. Fronts AO obtained by solving (5.3) and (5.4) for $dR = 100$ and $dA = 0$.

necting n rolls and $n + 2$ rolls can evolve from localized n (or $n + 2$) rolls in a long channel with rigid sidewalls. Suppose that, for instance, two rolls are localized in a channel with $As \sim 2.9$. A-mode and B-mode represent two rolls and four rolls, respectively. If three rolls are suppressed for some reasons, two rolls would propagates with a relatively negative velocity on the left edge of the two rolls region and four rolls evolve on the right edge. As a result, a defect is predicted to form as in Fig. 12(b). Similarly, if four rolls are localized initially, they propagate to the right with a positive velocity and two rolls would evolve on the left edge. We would see a defect as in Fig. 12(d).

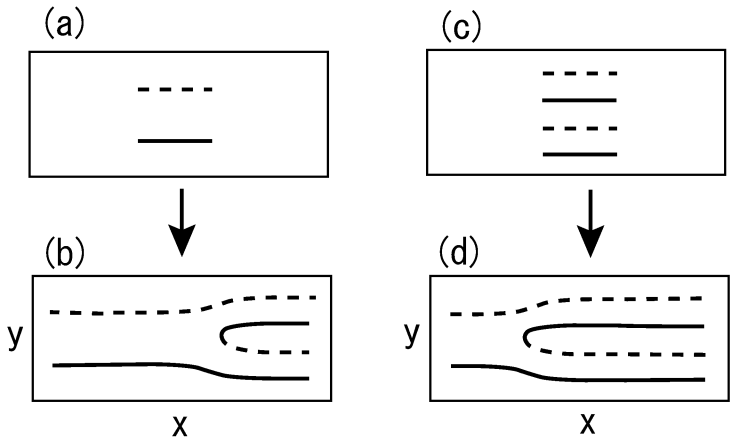

Figure 12. Sketches of a planform. The solid and dashed lines denote axes of counter-rotating rolls. (a) and (c) show initially localized rolls, (b) and (d) defects in a conjecture.

References

[1] T. Ogawa: RIMS Kokyuroku **1485** (2006) 33; T. Okuda & T. Ogawa: Math. Soc. Jpn. 2006 Autumn Meeting.
[2] L. D. Landau & E. M. Lifshitz: *Quantum Mechanics (Non-relativistic Theory)* (Butterworth Heinemann, 1977), Sec. 79.
[3] M. Ida: *Phys. Rev. E.* **72** (2005) 036306.
[4] G. Richardson: *Quart. Appl. Math.* **58** (2000) 685.
[5] C. P. Jackson & K. H. Winters: *International J. Numer. Methods Fluids* **4** (1984) 127.
[6] K. A. Cliffe & K. H. Winters: *J. Comput. Phys.* **67** (1986) 310.
[7] J. Mizushima & T. Nakamura: *J. Phys. Soc. Jpn.* **71** (2002) 677.
[8] Y. Kato & K. Fujimura: *J. Phys. Soc. Jpn.* **75** (2006) 034401.
[9] J. K. Platten & J. C. Legros: *Convection in Liquids*, (Springer, 1983), Chap. VIII, Sec. 4.
[10] M. van Hecke, C. Storm & W. van Saarloos: *Physica D* **134** (1999) 1.
[11] G. Dee & J. S. Langer: *Phys. Rev. Lett.* **50** (1983) 383.
[12] W. van Saarloos: *Phys. Rev. Lett.* **58** (1987) 2571; *Phys. Rev.* **A37** (1988) 211.